5.1 Introduction

The application of aerogel is found in various field however, it has gained interest in the field of functional aerogel development through incorporation of functional compounds (bioactive compounds, quantum dots, nanoparticles, etc.). Carbon dots (CDs) are very popular nanomaterials (< 10 nm) in the field of functional aerogel development as it possess superior qualities like high dispersibility in water and other polar solvents, high photostability, high biocompatibility, low photobleaching, low cytotoxicity, low chemical toxicity, and high fluorescence quantum yield (QY) (Jorns and Pappas, 2021). Moreover, the tunable fluorescence (excitation dependent) and versatile surface chemistry of carbon dots have extended its application potential (De Medeiros et al., 2019; Pappalardo et al., 2020). Bottom-up and top-down method are the two different route of CDs synthesis (Ozyurt et al., 2023; Adeola et al., 2023). The break down and peeling of carbon rich structures (carbon nanorods, carbon nanotubes, graphite, etc.) through electric arc discharge, laser ablation, chemical oxidation, etc. leads to synthesize CDs through top-down method. Whereas, the bottom-up method synthesize CDs from small carbon rich molecules like ethylene glycol, citric acid, etc. through pyrolysis, microwave heating, combustion, hydrothermal synthesis, etc. (Sharma and Das, 2019). Dehydration, polymerization, carbonization, and passivation are the processes involved in the synthesis of CDs. Moreover, the synthesis of CDs is now shifting towards the sustainable sources like bio-waste (vegetable peel, fruits peel, etc.) which is economic and easily available (Hu et al., 2014; Anuar et al., 2021). The parameters like, temperature, pH, solvent, etc. can change the photoluminescence behaviour of CDs (Vervald et al., 2025). The synthesized CDs are loaded into the aerogel to enhance the functionality of aerogel. CDs is loaded either prior to aerogel formation or post aerogel formation. In the process of prior addition of CDs, previously synthesized CDs were directly added to the precursor of aerogel or precursor of CDs was added to precursor of aerogel to develop CDs loaded aerogel. Whereas in the process of post addition of CDs, previously developed CDs were loaded directly into the aerogel matrix. The CDs loaded aerogel can response to different stimuli (pH, temperature, humidity, etc.) depending upon the characteristics of CDs and the aerogel (Zhang et al., 2020). Therefore, the CDs loaded aerogel with the superior qualities of both CDs and aerogel found broad range of applications like, photosensitizer (Wang et al., 2018), energy storage device

(Sun et al., 2021), air pollutant sensing system (Prinz and Richter, 2022; Wu et al., 2019), heavy metal detection system (Jing et al., 2022; Dolai et al., 2017), etc.

CDs loaded aerogel grabs the attention of food researchers for its application potential in food. Few group of researcher have developed CDs loaded aerogel to detect Fe^{3+} (Wang et al., 2022), H_2O_2 (Wang et al., 2019), organophosphate pesticides (Hu et al., 2019), etc. Some other CDs loaded materials like hydrogel, films, etc. are also developed for desalination of water and treatment of waste water (Sharshir et al., 2020), safeguard the food in terms of packaging (Moradi et al., 2021; Koshy et al., 2021), etc. A limited number of studies are available in the development of multiresponsive CDs loaded bio-polymer based aerogel. Therefore, in this study, CDs loaded corn starch based aerogel was developed and applied for pH sensing.

5.2 Materials and methods

5.2.1 *Materials*

Native corn starch (amylose content: 13.32%) was purchased from LOBA CHEMIE PVT. LTD. Ethanol (C_2H_5OH: ≥ 99.5% purity) was purchased from Changshu Hongsheng Fine Chemical Co. Ltd. Calcium chloride ($CaCl_2$), citric acid monohydrate ($C_6H_8O_7 \cdot H_2O$), ammonium hydroxide (NH_4OH; 25 %), sodium hydroxide (NaOH), hydrochloric acid (HCl), silica gel, and glycerol were procured from Merck Life Science Private Limited (Mumbai, India).

5.2.2 *Development of CDs based aerogel*

The development of CDs based aerogel (**Fig. 5.1**) consists of three steps (i) synthesis of CDs, (ii) development of aerogel, and (iii) loading of CDs and development of CDs based aerogel. All these three steps involved were explained briefly in the following sections.

5.2.2.1 *Synthesis of CDs*

Hydrothermal method of synthesis as reported by Zhou et al. (2015) and Naksen et al. (2022) was followed with some modifications to synthesize nitrogen doped CDs. Citric acid monohydrate and ammonium hydroxide was used as precursor material of CDs and nitrogen respectively. In brief, 1.05 g of citric acid monohydrate was mixed with deionized (DI) water to dissolve it properly, then 2.68 mL ammonia solution was added to the solution and the volume was maintained to 50 mL by adding DI water. The mixture was kept in a magnetic stirrer at 450 rpm for stirring for 30 min. The mixture was then transferred to a Teflon lined autoclave and kept in a muffle furnace for heating at 200 °C for 5 h. The autoclave was cooled in room temperature and the solution was centrifuged (10000 rpm for 15 min) and filtered

through membrane filter to remove large impurities. Moreover, to check the impact of nitrogen doping, CDs without using ammonia were also synthesised by following aforementioned process. The fluorescence intensities of both the CDs were observed. The excitation wavelength was also fixed through studying the CDs samples at different excitation wavelength (300 to 400 nm). The CDs showing high fluorescence intensity was selected for further analysis. Then the CDs were obtained through freeze drying from the selected yellow solution containing CDs and used for further analysis.

5.2.2.2 Development of aerogel

The aerogel was developed by following the method described in Section **4.2.2**. Corn starch (7.5 % w/v) was mixed with distilled water to prepare a solution. The solution was gelatinized at 93 °C using a laboratory stirrer with stirring at 450 rpm for 20 min. Then, 6 mL 0.01 % $CaCl_2$ and glycerol (5 %) was added to the gelatinized solution and stirred at 10000 rpm for 10 min. The solution was poured into cylindrical polypropylene mold and incubated at 4 °C for 2 days. The cylindrical shaped hydrogel was cut into small pieces (5 mm) and submerged into 30 to 100 % ethanol solution for ethanol substitution and to form alcogel. The alcogel were dried in a microwave oven (240 W for 280 min) to develop aerogel. The developed aerogel were stored in a desiccator (desiccant: silica gel) for further use.

5.2.2.3 *Loading of CDs and development of CDs based aerogel*

The individual aerogel samples were dipped into varying concentration of 5 mL CDs solution (0.5, 1.0, 2.0, 3.0, and 4.0 wt %) for overnight to get the CDs loaded into the aerogel matrix (**Fig. 5.2**) (Wu et al., 2019). The wet aerogel obtained after soaking was kept in a freezer at -18 °C for 16 h. Then the frozen samples were dried through sublimation using a freeze drier (-50 °C for 3 h). The developed CDs based aerogel were stored properly in an amber color desiccator (desiccant: silica gel) for further experiments and characterization.

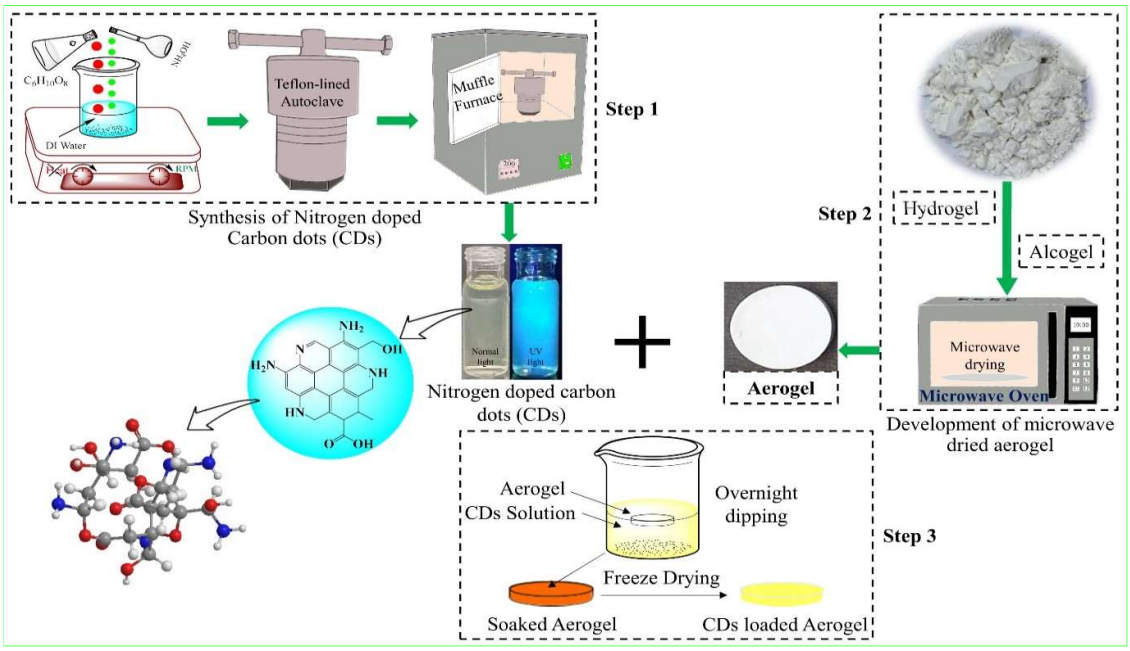

Fig. 5.1 Development process of carbon dots (CDs) based aerogel

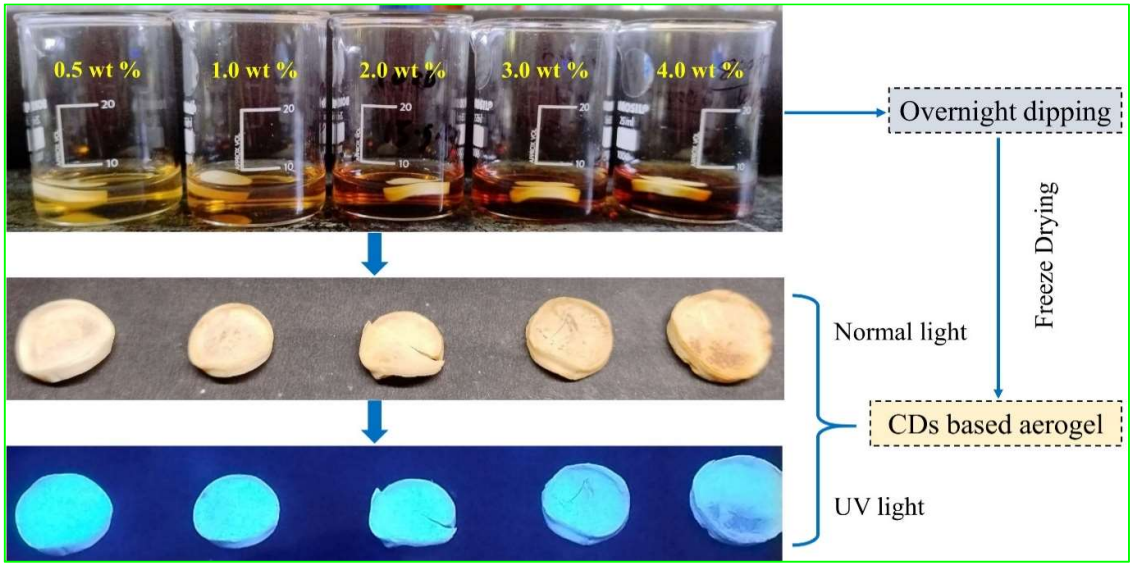

Fig. 5.2 Loading of different concentration of carbon dots (CDs) in aerogel

5.2.3 *Characterization of CDs*

5.2.3.1 *Concentration and yield*

The concentration and yield of CDs after freeze drying was calculated using the following equations (**Eq. 5.1** and **Eq. 5.2**):

$$\text{Concentration}\left({}^{\text{mg}}/_{\text{L}}\right) = \left(\frac{\text{Weight of Freeze dried CDs (mg)}}{\text{Initial Volume of CDs solution(mL)}}\right) \times 1000 \qquad (5.1)$$

$$\text{Yield}(\%) = \left(\frac{\text{Weight of Freeze dried CDs}}{\text{Initial weight of CDs solution}}\right) \times 100 \quad (5.2)$$

5.2.3.2 *Quantum yield*

The quantum yield (QY) of CDs was measured with reference to a standard i.e. quinine sulphate dissolved in 0.1 M H_2SO_4. The QY was calculated at 330 nm excitation wavelength using following equation (**Eq. 5.3**) (Dhenadhayalan et al., 2016; Schneider et al., 2017):

$$QY_{CDs}(\%) = QY_S \times \left(\frac{A_S}{A_{CDs}}\right) \times \left(\frac{I_{CDs}}{I_S}\right) \times \left(\frac{\eta_{CDs}}{\eta_S}\right)^2 \quad (5.3)$$

Where subscripts CDs and S refers to Carbon dots and standard respectively, A is the absorbance, I is the integrated fluorescence intensity, and η is the refractive index. Refractive index of water and 0.1 M H_2SO_4 is 1.33. QY_S = 0.54.

5.2.3.3 *FTIR, UV-vis, Fluorescence, and NMR spectra*

To explore the functional group present in the CDs, FTIR spectroscopy was performed using a spectrophotometer (Nicolet Instruments 410 FTIR, Thermo Scientific, USA). The KBr pellet method was used to prepare the sample. The spectroscopy was performed in the wavenumber range from 4000 to 400 cm^{-1} (Zattar et al., 2021).

The UV-Visible spectroscopy of CDs solution (5.89, 2.94, and 0.59 g/L) was done on UV-Vis spectrometer (Orion AquaMate 8100, Thermo Fisher Scientific, USA). The range of scanning was set from 200 nm to 800 nm to check the π-π transitions in the developed CDs (Himaja et al., 2015).

Fluorescence spectroscopy was performed in a fluorescence spectrophotometer (Cary Eclipse, Agilent, USA). The CDs solution (5.89, 2.94, and 0.59 g/L) was excited at 330 nm wavelength and the emission spectra was recorded in the range of 200 to 800 nm (Zhou et al., 2015). Moreover, fluorescence spectroscopy was also performed in CDs solution, concentration ranges from 10 to 5890 mg/L to study the fluorescence behaviour corresponds to changing concentration. The corresponding fluorescence intensities were noted.

To know the chemical structure, chemical shifts, surface functionalities, etc. of CDs NMR spectroscopy was performed by dissolving CDs in D_2O. The ^{13}C-NMR and ^{1}H-NMR spectra was obtained using ECS-400 MHz NMR spectrometer (JEOL, Japan). The chemical shifts (in

parts per million: ppm) of ^{1}H-NMR was measured in reference with the residual peak of D_2O (^{1}H = 4.66 ppm) (Mohammed et al., 2023).

5.2.3.4 Morphology

Transmission electron microscopy (TEM) was performed to characterize the particle morphology of CDs. The solution of CDs was mixed with ultrapure water and dropped the mixture onto a super-thin carbon coated copper grid (200 meshes). The excess solvent is evaporated prior to take TEM images. A high resolution Transmission electron microscope (TECNAI G2 20 S-TWIN, FEI COMPANY, USA) operated at 200 KV of accelerating voltage was used to obtain the TEM images at 150,000 × magnification (Gao et al., 2017). The obtained images were processed through Image J software to obtain particle size distribution of CDs. The single area diffraction (SAED) pattern was also obtained to reveal the crystalline behaviour of CDs. The polydispersity index (PDI) was calculated by using following equation (**Eq. 5.4**) (Cailotto et al., 2018):

$$\mathrm{PDI} = \left(\frac{\sigma}{d}\right)^2 \tag{5.4}$$

Where, σ is standard deviation of the measured diameter and d is mean particle diameter.

5.2.4 *Characterization of CDs based aerogel*

5.2.4.1 *Loading content of CDs*

The loading can be directly measured through gravimetric approach, which is mostly used in calculating the loading value of CDs. Mass difference between the aerogel after and before loading was calculated to get the loading value (An et al., 2025; Wu et al., 2019). In this study the similar concept of mass difference was used in another way by the means of volume of CDs solution absorbed by the sample multiplied by concentration of CDs solution. The volume of CDs absorbed by individual aerogel was calculated by subtracting the volume of CDs solution remained (V_R) after soaking from the initial volume of CDs (V_I). The loading content of CDs was calculated by following **Eq. 5.5:**

$$L_{CDs}\left(\mathrm{mg}/\mathrm{g}\right) = \frac{(V_I - V_R) \times C_{CDs}}{m_A} \tag{5.5}$$

Where, L_{CDs} is the loading content of CDs, ($V_I - V_R$) is the volume (mL) of CDs absorbed, C_{CDs} is the concentration (mg/mL) of CDs solution, and m_A is the weight (g) of aerogel before soaking.

5.2.4.2 *Fluorescence spectra and Green/Blue (G/B) value*

Fluorescence spectroscopy was performed in a fluorescence spectrophotometer (Cary Eclipse, Agilent, USA). The CDs based aerogel were excited at 330 nm wavelength and the emission spectra was recorded in the range of 200 to 800 nm. The corresponding fluorescence intensities were noted.

The CDs based aerogel were kept under UV light (wavelength: 365 nm) for emitting fluorescence color as a result of excitation. The images of the fluorescence emitting aerogel were taken by a smart phone camera. The images were processed through Image J software to obtain green-blue (G-B) value out of those. The G/B value was calculated from the GB data.

The optimum concentration of CDs in aerogel was selected on the basis of fluorescence intensity and Green / Blue (G/B) of the obtained images of CDs based aerogel under UV light (wavelength: 365 nm).

5.2.4.3 *FTIR, XRD, and DSC spectra*

FTIR of CDs based aerogel was performed to observe the covalent reaction between aerogel and CDs. Aerogel was crushed with a motor pastel to make fine powder. Then the powdered aerogel was mixed with KBr to form a KBr pellet. FTIR spectrophotometer (Nicolet Instruments 410 FTIR, Thermo Scientific, USA) was used to perform FTIR spectroscopy in the wavenumber range from 4000 to 400 cm^{-1} (Wu et al., 2019).

The aerogel samples were exposed to an X-ray beam at 15 mA and 30 kV using an X-ray diffractometer (Miniflex, Rigaku Corporation, Japan). The diffraction angle (2Θ) range was set to 5° to 80° with a step angle of 0.05°. The crystallinity index (CI) or degree of crystallinity was determined through analysis of the diffraction pattern (Kumar et al., 2020).

Thermal properties of the CDs based aerogel were determined using a differential scanning calorimeter (DSC 214, NETZSCH, Germany). The sample (5 mg) was loaded into an aluminum pan without the addition of water and was sealed for thermal scanning. Thermal scanning was performed in the temperature range of 25 to 400 °C, under a nitrogen purge (20 ml/min), at a heating rate of 10 °C/min (Franco et al., 2018). A DSC thermogram was obtained after analysis which was used to calculate the onset, peak, and end temperature.

5.2.4.4 *pH dependent behaviour of CDs based aerogel*

The pH of CDs was measured using a pH meter (EUTECH pH 700, Thermo Fisher Scientific, USA). The pH of CDs solution was tuned and maintained to 3, 6, 9, and 12 by adding

0.1 N HCl and 0.1 N NaOH solution. The aerogel were loaded with CDs solution of different pH (3, 6, 9, and 12) by dipping the aerogel in respective CDs solution. The images of wet aerogel under UV light (wavelength: 365 nm) were taken and G/B values were obtained using Image J software. A linear fitted calibration curve was drawn to build relation between pH and G/B value. The CDs loaded aerogel was spiked with CDs solution of known pH, then the image of spiked aerogel was taken under UV light (wavelength: 365 nm) to obtain G/B value and the obtained value of pH from the calibration curve was compared with the spiked pH value. The compatibility of the CDs loaded aerogel as pH sensor was observed (M J et al., 2025).

5.2.5 *Statistical analysis*

All the analyses were performed in triplicates and the results data were represented as mean ± standard deviation. Statistical analysis was performed using SPSS software (SPSS 17.0, SPSS Inc., Chicago, IL). The data were analyzed by one-way analysis of variance test and to determine the significant differences among individual results DUNCAN's multiple range test (DMRT) ($p < 0.05$) was performed. The level of significance was set to $p < 0.05$ to determine the statistical significance. Microsoft Excel 2017 and Origin Pro 2018 (OriginLab, USA) were used for graphing and principal component analysis.

5.3 Results and discussion

5.3.1 *Synthesis and characterization of CDs*

CDs were synthesized by reactions of citric acid monohydrate and ammonium hydroxide (nitrogen precursor). A highly increased fluorescence intensity was observed (**Fig. 5.3a**) for the CDs synthesised with nitrogen precursor as compared to the CDs synthesised without nitrogen precursor (**Fig. 5.3b**) which supports the nitrogen doping in CDs. The citric acid forms a close framework through self-assembly as a consequence of intermolecular dehydration. The dehydration and condensation reaction of – COOH and – NH_2 forms amide under the action of nitrogen source. Then the intermolecular dehydration of amide with the adjacent carboxyl group forms pyrrolic N. As the reaction continues more number of N enters into the framework and the nitrogen doped CDs are formed. Due to the ammonia structure, amino group was contained in CDs and a five membered N-doped ring is developed (Qu et al., 2014; Zhu et al., 2021). The carbonization of precursor occurred at 200 °C results in formation of CDs. Citric acid reacted with ammonia to develop a citrazinic acid fluorophore (Schaber et al., 2004). Alongside the carbonization reaction, citric acid can underlie intramolecular condensation and cyclization to form derivatives of citrazinic acid as it contains three carboxyl functionalities

(Schneider et al., 2017). The excitation wavelength was also selected to 330 nm based on the highest stokes shift observed. A pale yellow colored solution containing CDs was obtained after synthesis. The concentration and yield of CDs obtained was 5.89 g/L and 0.60 % respectively. The low synthesis yield obtained in hydrothermal synthesis was supported by the investigation reported by Crista et al. (2020) for the hydrothermal synthesis of CDs using citric acid and urea as precursor.

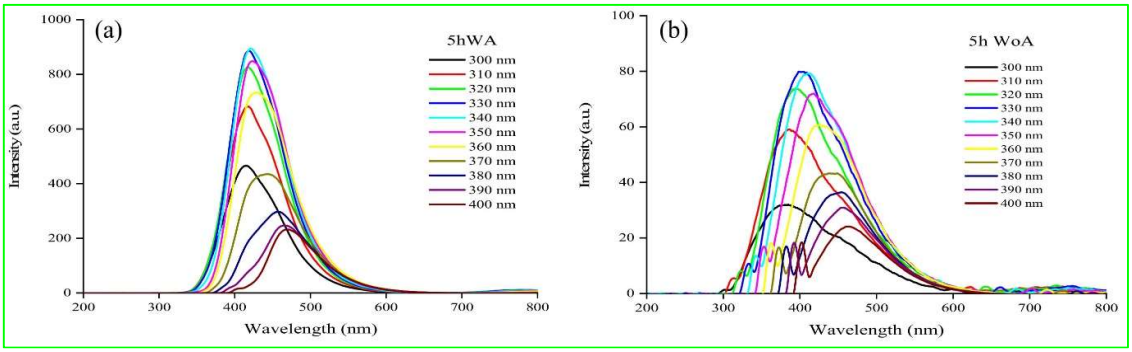

Fig. 5.3 Fluorescence spectra of CDs developed with ammonia (WA) (a) and without ammonia (WoA) (b)

Photoluminescence of CDs is characterized by QY. QY is a significant parameter of carbon based nanomaterials which regulates their application potential in various field. Therefore, a high QY (> 30 %) is always desired (Qu et al., 2014). Nitrogen doping serves as an effective way of enhancing QY (Qu et al., 2014; Ding et al., 2014). The QY of CDs was found approximately 46 % which showed a comparable result to other studies performed by different group of researcher (Wang et al., 2018; Zhu et al., 2021). The diluted CDs solution exhibit strong blue fluorescence under UV-light (365 nm) although it is of slight yellow color under visible light (**Fig. 5.4a**).

FTIR is performed to study the presence of functional group of CDs (**Fig. 5.4b**). The strong absorption band observed at 3468 and 3244 cm^{-1} may be ascribed to O-H and N-H stretching respectively (Zhu et al., 2021). The absorbance band found in this region for the citric acid monohydrate solution (precursor solution of CDs) was weak as compare to synthesised CDs solution (CDS). The improvement in stability and hydrophilic nature of CDs in aqueous solution was supported by O-H and N-H functional groups (Zhu et al., 2021). The extended shoulder observed near 2925 cm^{-1} ascribed to C-H stretching vibrations (Wang et al., 2018). The strong and broad peak observed at 1639 cm^{-1} in CDS as compare to CAS may ascribed to C=O stretching vibrations that suggested more ring formation by carbons (Zhu et al., 2021).

This region also suggested C=C and/or C=N stretching vibrations which confirms the presence of aromatic domains (Meierhofer et al., 2020). The absorption band near 1560 cm^{-1} amalgamated to C=C stretching vibrations and $–NH_2$ bending vibrations. A sharp peak was observed at 1400 cm^{-1} which suggests C-N band stretching that supports nitrogen doping in CDs (Wang et al., 2018). The peak near 1159 and 1052 cm^{-1} ascribed to C–O stretching vibrations which indicates the presence of ample number of O-containing groups (Chen et al., 2014; Wang et al., 2018).

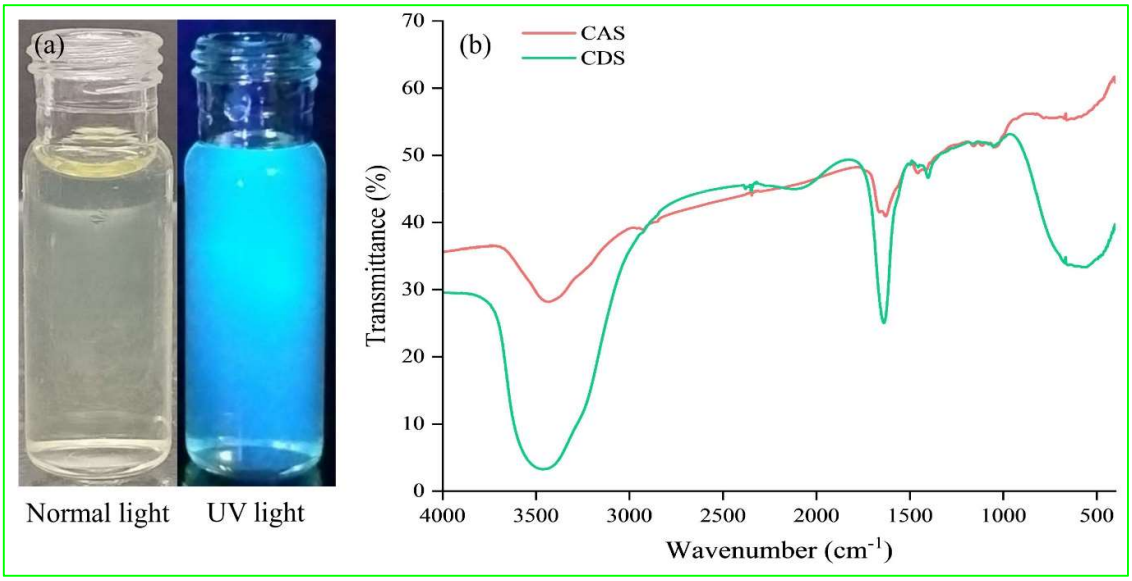

Fig. 5.4 Fluorescence behaviour (a) and FTIR spectra (b) of the developed CDs

Note: CAS: Citric acid monohydrate solution, CDS: Carbon dots solution

In the UV-Spectra (**Fig. 5.5a**) of CDs solution, a strong absorption peak was observed near 330 nm. This absorption shoulder is associated with the n-π* transition of C=O bonds or others which indicates the existence of carbonyl or conjugated carbonyl groups (Zhou et al., 2015; Wang et al., 2018). However, a peak nearly at 270 nm was also observed which suggests π-π* transition of the conjugated C=C bonds analogous to carbon-core (Dhenadhayalan et al., 2016). More specifically, the n-π* transition originates from the lone pair electrons of oxygen groups located on the particle surface (Vallan and Imahori, 2022). The absorption peak also confirms the presence of specific functional group (C=O) in CDs. The concentration of CDs solution showed an impact on the absorption spectra (**Fig. 5.5a**). As the concentration reduced the absorption peak is also reduced.

The fluorescence spectra (**Fig. 5.5a**) of CDs solution were observed at an excitation wavelength of 330 nm. At an emission wavelength of approximately 420 nm, the peak intensity of 5.89 g/L CDs solution was found to be 32.02 a.u. whereas, the peak intensity observed in 2.94 g/L and 0.59 g/L CDs solution 152.48 and 999.92 a.u. respectively. This is a common phenomenon which contributes to the surface states which affects the band gaps of CDs. The quantum dimensions and molecular state of CDs contributes to the complexity of its excitation (Zhou et al., 2015). The widely accepted mechanism of fluorescence is the radiative recombination of electron-hole pairs (Dhenadhayalan et al., 2016). The increase in concentration exhibited increase in fluorescence intensity followed by a decrease (**Fig. 5.5b**). The increase may be due to increase in the number of fluorophore however, the decrease be due to lacking of free space required to release energy in the form of fluorescence by the fluorophore as a consequence of overcrowd.

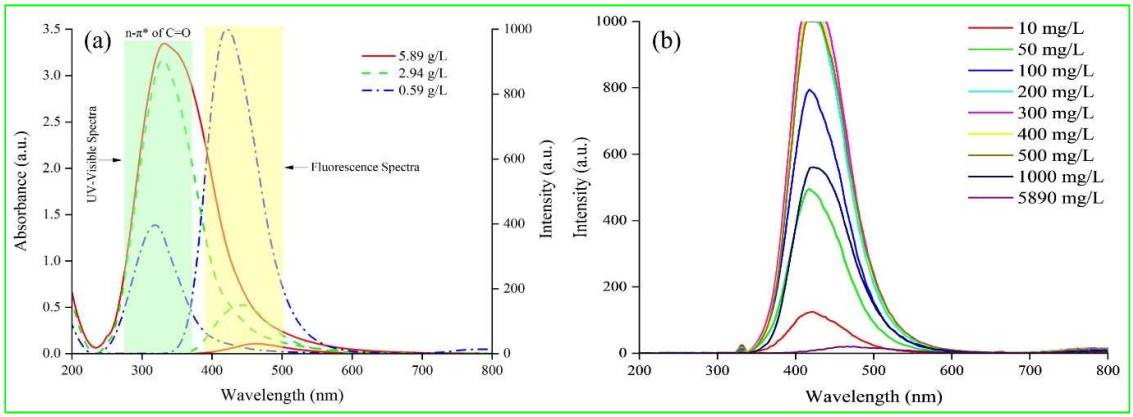

Fig. 5.5 UV and fluorescence spectra of CDs solution (a) and fluorescence spectra at different concentration of CDs (b)

The NMR spectra (C-NMR and H-NMR) was obtained through NMR spectroscopy to confirm the chemical shifting and surface functionalities of CDs (**Fig. 5.6** and **Fig. 5.7**). The presence of sp^2 and sp^3 carbon atoms in CDs was confirmed by the C-NMR spectra (**Fig. 5.6a**). The peaks in the range from 170 to 185 ppm indicates the sp^2 carbons with carbonyl nature which may be ascribed to existence of amide or carboxylic groups (Sk and Chattopadhay, 2014). Whereas, the aliphatic sp^3 carbon atoms were indicated by the peak ranged from 30 to 45 ppm (Sk and Chattopadhay, 2014). The CDs solution showed two additional peak in between 30 to 50 ppm as compare to precursor solution which showed only one peak in that range. However, the precursor solution of CDs showed an additional peak at approximately 74 ppm which may suggests the presence of C–OH or C–O–C aliphatic sp^3 carbon atoms (**Fig.**

5.6b). The presence of C–H, C=C and other sp^2 carbon atoms, and C=O were indicated by the peak ranged from 1 to 3, 6 to 8, and 8 to 10 ppm respectively in the H-NMR spectra (**Fig. 5.7**) (Tiwari et al., 2023). The H-NMR spectra of CDs solution exhibited ample number of peaks in the range of 1 to 3 ppm and it also exhibited few peaks in the range from 6 to 10 ppm (**Fig. 5.7a**). Whereas, the CDs precursor solution displayed only four peaks in the range from 1 to 3 ppm and few peaks very close to the peak of D_2O (**Fig. 5.7b**).

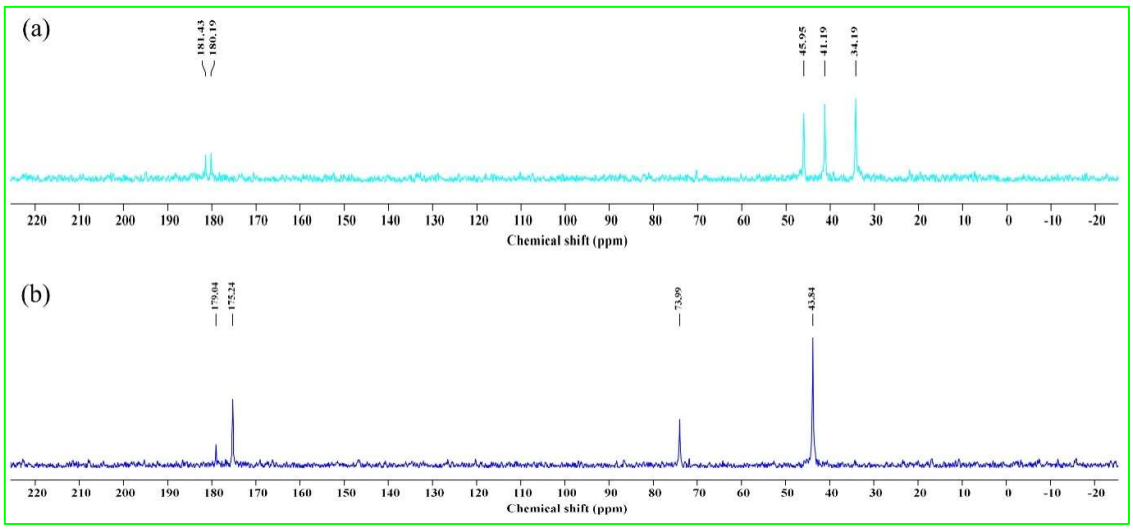

Fig. 5.6 C-NMR spectra of CDs solution (a) and CDs precursor solution (b)

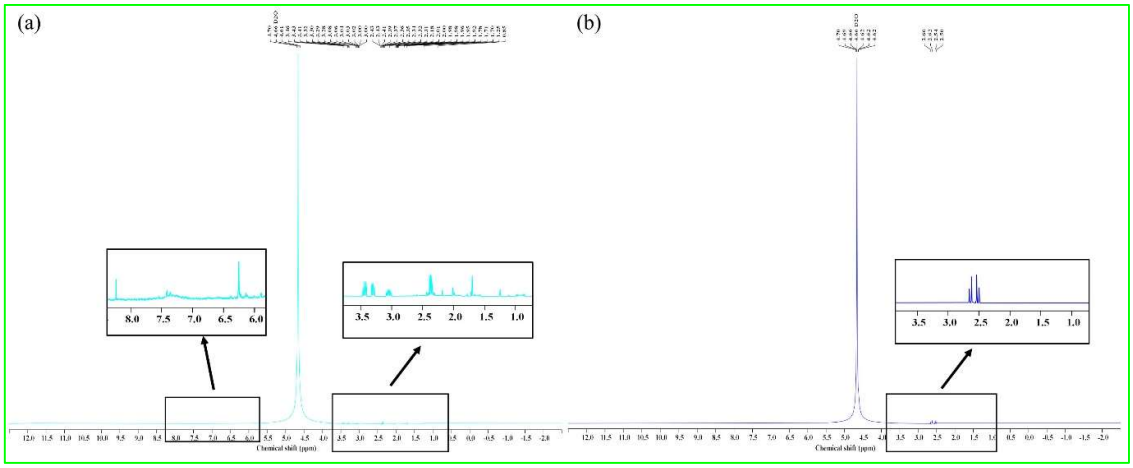

Fig. 5.7 H-NMR spectra of CDs solution (a) and CDs precursor solution (b)

The TEM images (**Fig. 5.8**) showed that the particle size of CDs ranges from 0.719 to 5.906 nm with mean diameter of 2.21 nm. Although a wide range of particle size observed, most of the particles size between 1 to 4 nm which can be considered as narrow size distribution. TEM images (**Fig. 5.8**) and particle size distribution graph (**Fig. 5.8a**) suggested that the CDs

particles were mono-dispersed with a PDI value of 0.21 as particles having PDI value of less than 0.2 is typically considered as mono-dispersed which indicates non aggregated narrow size distribution (Ezati et al., 2022). The SAED pattern (**Fig. 5.8b**) showed that the CDs lacks ring or spots which suggests that CDs exhibited amorphous nature (Lu et al., 2012; MJ et al., 2025).

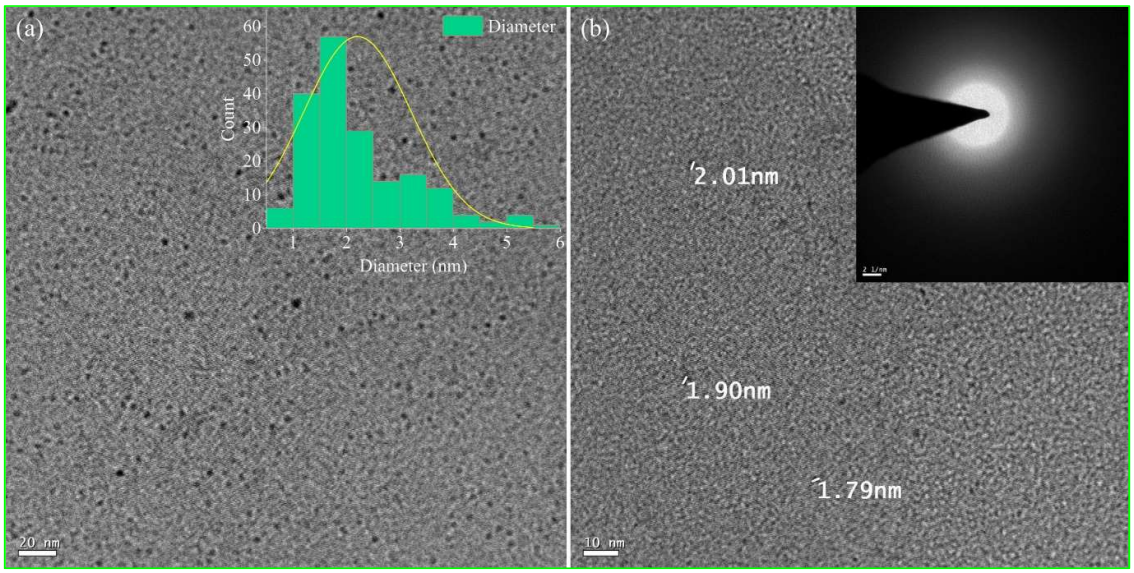

Fig. 5.8 TEM images, particle size distribution (a) and SAED pattern (b) of CDs

5.3.2 *Development and characterization of CDs based aerogel*

The appearance of CDs based aerogel was shown in **Fig. 5.9**. The fluorescence behaviour of the developed aerogel was observed under UV light (wavelength: 365 nm). Apparent blue fluorescence was exhibited by all the aerogel loaded with CDs, which proved that the original fluorescence was maintained even after loading of CDs into aerogel. However, no fluorescence was exhibited by the control sample which was not loaded with CDs (**Fig. 5.9**). The highest quantity of loaded CDs was observed in 4 wt % CDs based aerogel with the loading value 59.66 mg/g of aerogel however, the lowest loading value (6.67 mg/g of aerogel) observed in 0.5 wt % CDs based aerogel (**Fig 5.10a**). The CDs loading content in aerogel is a crucial factor in the determination of fluorescent behaviour and its potential application. The study performed by Wu et al. (2019) reported loading value through UV-absorbance and gravimetric method, both the method showed similar result with non-significant difference.

The G/B value and fluorescence spectra of aerogel was further used to evaluate the fluorescence characteristics of aerogel. The G/B value of all the CDs based aerogel is showed in **Fig. 5.10a**. It was observed that the G/B value was increased very minimally with the increase in concentration of CDs solution till 1.0 wt %, after this a gradual increase was

observed for 2.0 wt % however, the increase was non-significant and beyond this concentration a significant decrease in G/B value was observed. The fluorescence spectra of all the CDs based aerogel was displayed in **Fig. 5.10b**. The fluorescence intensity of 0.5 and 1.0 wt % CDs based aerogel was almost constant. The fluorescence intensity of 2.0 wt % CDs based aerogel was higher however, the increase was non-significant. Beyond this concentration, a sharp decrease in fluorescence intensity was observed. This findings supports the observation of G/B value. As the significant decrease in both G/B value and fluorescence intensity observed immediate after 2.0 wt % CDs therefore, this concentration of CDs was avoided and 1.0 wt % CDs was selected as the optimum concentration of CDs for the CDs based aerogel development for further characterization and application.

The uniformity of CDs loading was observed by the fluorescence images obtained from the transversely and vertically cut cross-sections of CDs (1 wt %) based aerogel. Similar fluorescence was observed from all cross-sections as exhibited by the surface of CDs based aerogel (**Fig. 5.11a**) which confirmed the uniform dispersibility of CDs in the aerogel matrix. Moreover, the stability of CDs in the aerogel matrix was observed by immersing the crushed CDs based aerogel powder in water for 3 h for any possible quenching of fluorescence and leakage of free CDs. The fluorescence images (**Fig. 5.11b**) of the immersed aerogel and supernatant water showed no change in color even after the end of experiment. The G/B values obtained (**Table 5.1**) from the images of immersed aerogel and supernatant water before and after the experiment, showed negligible differences which confirmed that the developed CDs based aerogel have retained its stable fluorescence behaviour possibly due to no leakage of CDs (Wu et al., 2019).

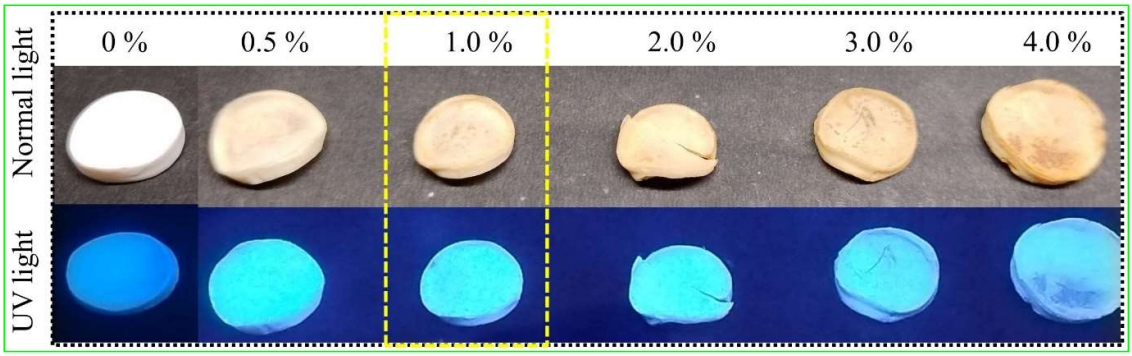

Fig. 5.9 Appearance and fluorescence nature of the developed aerogel

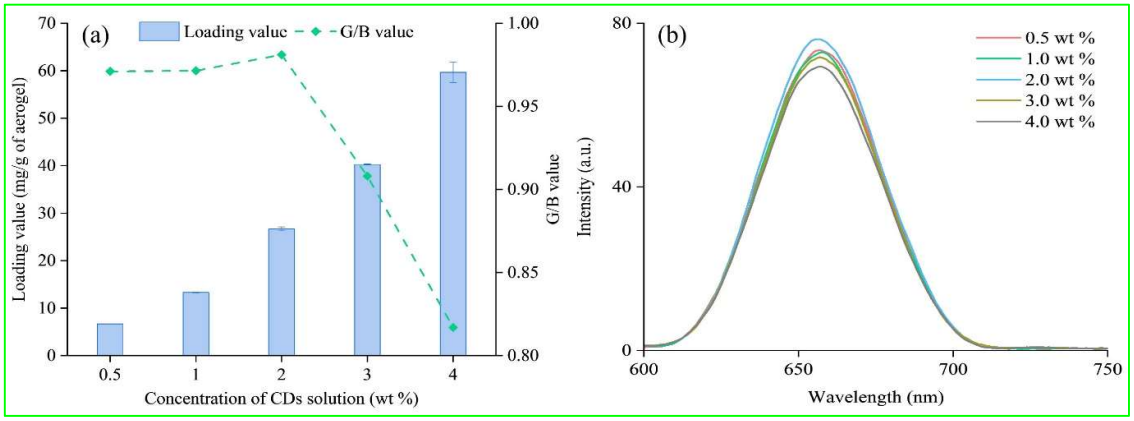

Fig. 5.10 Loading value and G/B (green/blue) value (a) and fluorescence spectra (b) of the developed CDs based aerogel

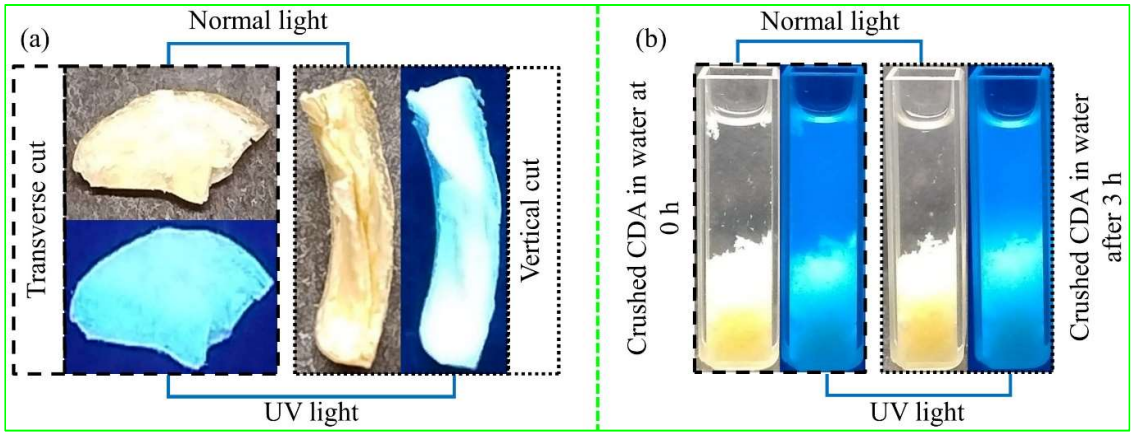

Fig. 5.11 Cross-sectional images of transversally and vertically cut aerogel (a) and crushed carbon dots based aerogel (CDA) in water (b)

Table 5.1 G/B values of crushed aerogel immersed in water and supernatant water

Time (h)	G/B value of crushed aerogel	G/B value of supernatant water
0	0.5169 ± 0.0019	0.9977 ± 0.0109
3	0.5174 ± 0.0025	1.0105 ± 0.0015

The FTIR spectra of CDs loaded aerogel and control aerogel was examined (**Fig. 5.12**) to observe the existence of functional groups. Both the aerogel exhibited the characteristics pattern of corn starch. The peak near 2930 cm^{-1} ascribed to C–H band stretching in both the aerogel (Jing et al., 2022). The $–NH_2$ stretching at 1560 cm^{-1} of CDs was observed at 1576 cm^{-1} (exists as extended shoulder) in the CDs based aerogel spectra (Wu et al., 2019; Jing et al., 2022). The wide region at 1650 cm^{-1} suggests the existence of −CO−NH− stretching as

exhibited by the CDs solution (Wu et al., 2019). The observed band stretching vibrations confirms the linkage between CDs and aerogel.

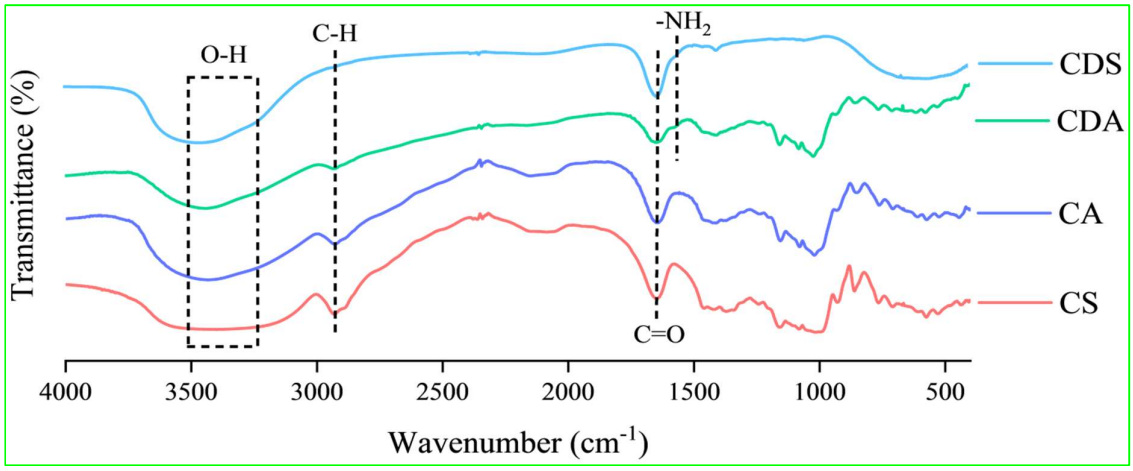

Fig. 5.12 FTIR spectra of CS (corn starch), CA (control aerogel without CDs), CDA (CDs based aerogel), and CDS (carbon dots solution)

X-Ray diffraction pattern of CDs based aerogel (CDA) and control aerogel (CA) without addition of CDs was shown in **Fig. 5.13**. Major diffraction peak in CDA was observed (**Fig. 5.13**) at about 2Θ = 17, 19, 21, 23° along with a minor peak at about 2Θ = 34°, which suggested a crystalline structure same as the aerogel without CDs. However two additional small peak was observed at 2Θ = 12 and 13° however, in the case of control aerogel it was observed in the form of a broad sharp peak at 2Θ = 13°. The crystalline integrity of the aerogel was affected by the addition of CDs which is supported by crystallinity index (CI) value of both the aerogel (control aerogel: 39.08 % and CDs based aerogel: 37.17 %). This may be due to presence of amorphous CDs inside the aerogel matrix. No major changes in the diffraction pattern was observed before and after addition of CDs which concludes that loading of CDs showed less influence on the basic structure of aerogel (Xu et al., 2022).

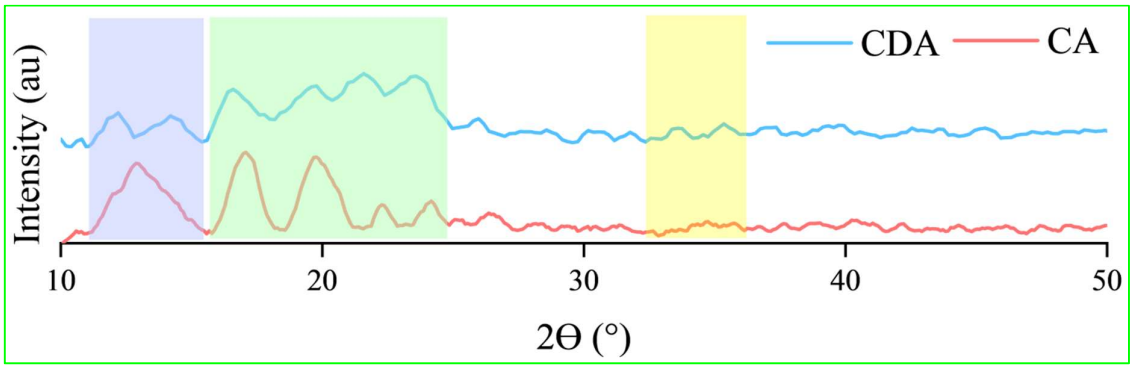

Fig. 5.13 X-Ray diffraction pattern of CA (control aerogel without CDs) and CDA (CDs based aerogel)

The thermogram (**Fig. 5.14**) obtained from differential scanning calorimetry (DSC) experiment was used to explain the thermal behaviour of the CDs based aerogel. The onset, peak and end temperature of the first endothermic peak of the aerogel was 40.3, 70.7, and 107.0 °C respectively. The end temperature was decreased drastically which suggest the decrease in formation of crystallites having higher melting point (Luo et al., 2006). The reduction in enthalpy of first endothermic peak (- 242.5 J/g) was observed as compare to control aerogel (- 282.3 J/g) which may be correlated with the decrease in end temperature. This finding is supported by the CI value of CDs based aerogel.

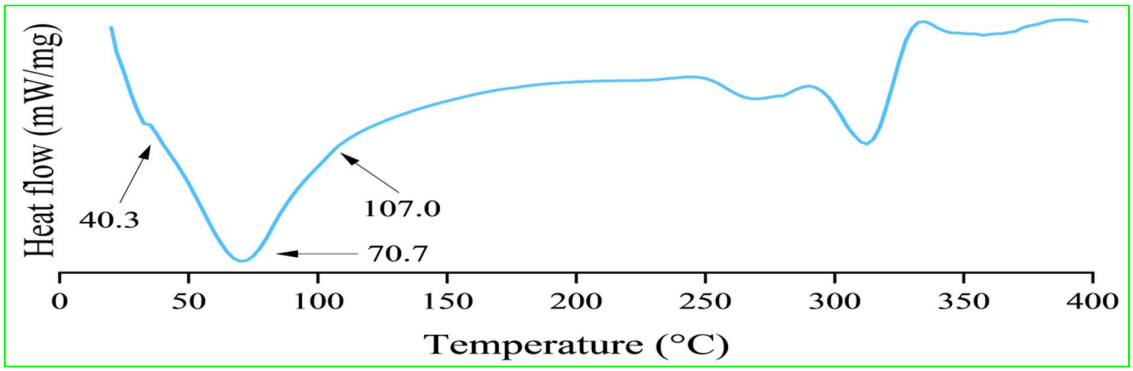

Fig. 5.14 DSC (differential scanning calorimetry) thermogram of CDs based aerogel

The G/B ratio reduces the influence of excitation intensity, camera exposure, sample concentration and optical path changes as the effect of all the factor in both G/B is similar and cancel each other (Xiao et al., 2023). This is how the G/B method give advantage in ratiometric fluorescence sensing. A camera pixel's RGB values represent the integrated intensity within the camera's red, green and blue sensitivities. The dominant components of CDs emission falls primarily into the blue and green sensitivities region of the camera. Therefore, the acquired G and B values are proportional to the relative emissive components and used quantitatively after calibration. The application of fluorescence color images into quantitative RGB ratios for metal and pH sensing is reported by several group of authors (Wei et al., 2021; Xiao et al., 2023). The G/B value of the obtained images of pH tuned CDs based aerogel and the corresponding pH to each aerogel was plotted (**Fig. 5.15**), which showed a linear relationship. With the increase in pH from 3 to 12, the decrease in G/B values were observed. The decrease in G/B value of the fluorescence color may be due to the effect of deprotonation with the increase in pH which changes the surface states of CDs (Meierhofer et al., 2020). The G/B value v/s pH

plot exhibited R^2 value of 0.9335. The relationship was validated through spiking with CDs solution of known pH (pH = 3) in a CDs based aerogel. The pH was obtained by putting the G/B value of the spiked sample in the linear equation of the plotted graph. The obtained pH (pH = 3.27) showed 9 % deviation from the spiked pH. Therefore, the CDs based aerogel can be used to determine unknown pH effectively.

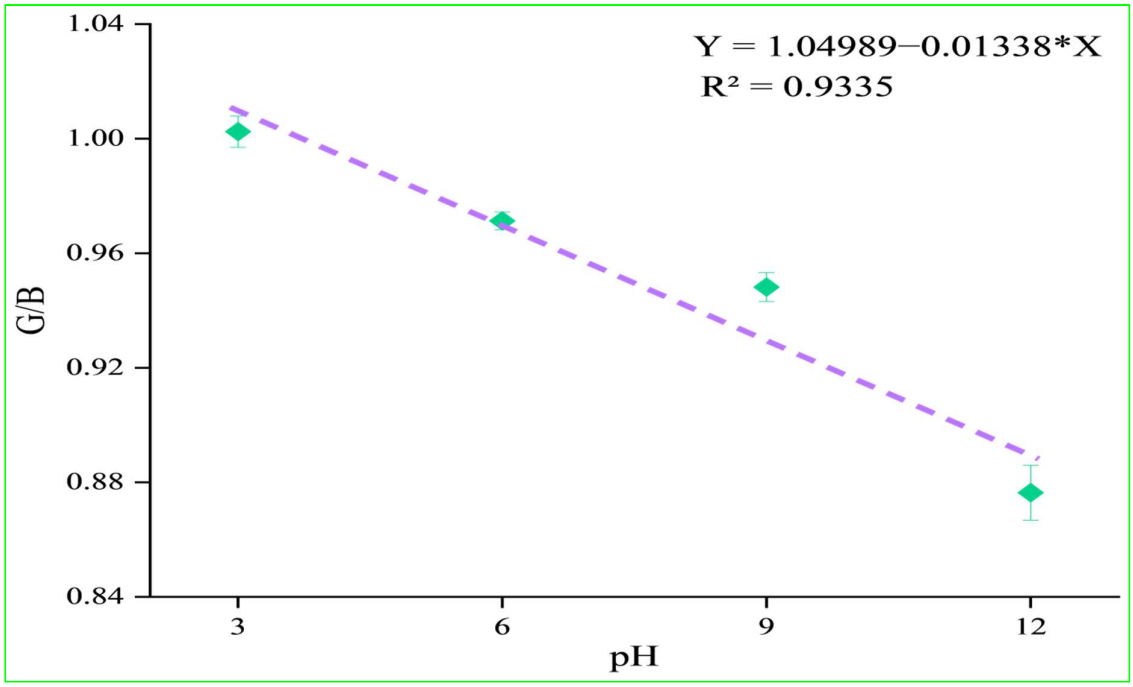

Fig. 5.15 Green/blue (G/B) value v/s pH relationship of CDs based aerogel

5.4 Conclusion

Carbon dots (CDs) were synthesised through hydrothermal method which showed good quality attributes (quantum yield, particle size, fluorescence, etc.). UV-absorbance, fluorescence intensity, morphology, etc. have studied to characterize the CDs. The addition of ammonia as nitrogen precursor have significantly improved the fluorescence characteristics of CDs which confirmed the nitrogen doping. The presence of $–NH_2$ and C–N stretching vibrations have supported nitrogen doping in CDs. CDs showed good emission characteristics (420 nm) at an excitation wavelength of 330 nm with a stoke shifts of 88.03 nm. The presence of sp^2 and sp^3 hybridized carbon atoms was confirmed by the NMR spectra. The average diameter of CDs was found as 2.21 nm with a PDI value of 0.21 which indicates mono-dispersed nature of CDs. The SAED pattern have confirmed the amorphous nature of CDs. Aerogel have developed using microwave drying approach. The CDs have loaded into aerogel matrix through overnight dipping into CDs solution. CDs loaded wet aerogel have dried

through freeze drying method. The 1.0 wt % CDs solution loaded aerogel was selected as optimum CDs based aerogel. The developed CDs based aerogel have retained stable fluorescence characteristics as exhibited by CDs. The CDs based aerogel showed uniformity in CDs dispersion inside the aerogel matrix. The FTIR spectra confirmed that the CDs based aerogel have retained both the native qualities of corn starch and CDs. The CDs based aerogel possessed good thermal characteristics and lesser crystallinity index value than the control aerogel. The CDs based aerogel was used as a pH sensing material through tuning the pH of CDs solution and loading it into aerogel matrix. The CDs based aerogel exhibited good results with a deviation of only 9% while determining pH through spiking approach. CDs based aerogel paves its way of application towards sensing due to its superior qualities related to sensing.

5.5 References

Adeola, A. O., Clermont-Paquette, A., Piekny, A., & Naccache, R. (2023). Advances in the design and use of carbon dots for analytical and biomedical applications. *Nanotechnology*, *35*(1), 012001.

An, R., Liu, J., Ma, H., Yan, Y., Guo, Y., Pan, Q., & Li, S. (2025). Fabrication of Wood-Derived Carbon Aerogel/Mg (OH) 2 Bio-Composite and Its High Performance for Adsorption and Separation of Cadmium Ions. *C*, *11*(2), 32.

Cailotto, S., Amadio, E., Facchin, M., Selva, M., Pontoglio, E., Rizzolio, F., Riello, P., Toffoli, G., Benedetti, A., & Perosa, A. (2018). Carbon dots from sugars and ascorbic acid: role of the precursors on morphology, properties, toxicity, and drug uptake. *ACS medicinal chemistry letters*, *9*(8), 832-837.

Chen, X., Jin, Q., Wu, L., Tung, C., & Tang, X. (2014). Synthesis and unique photoluminescence properties of nitrogen-rich quantum dots and their applications. *Angewandte Chemie*, *126*(46), 12750-12755.

Crista, D. M., Esteves da Silva, J. C., & Pinto da Silva, L. (2020). Evaluation of different bottom-up routes for the fabrication of carbon dots. *Nanomaterials*, *10*(7), 1316.

De Medeiros, T. V., Manioudakis, J., Noun, F., Macairan, J. R., Victoria, F., & Naccache, R. (2019). Microwave-assisted synthesis of carbon dots and their applications. *Journal of Materials Chemistry C*, *7*(24), 7175-7195.

Dhenadhayalan, N., Lin, K. C., Suresh, R., & Ramamurthy, P. (2016). Unravelling the multiple emissive states in citric-acid-derived carbon dots. *The Journal of Physical Chemistry C*, *120*(2), 1252-1261.

Ding, H., Wei, J. S., & Xiong, H. M. (2014). Nitrogen and sulfur co-doped carbon dots with strong blue luminescence. *Nanoscale*, *6*(22), 13817-13823.

Dolai, S., Bhunia, S. K., Zeiri, L., Paz-Tal, O., & Jelinek, R. (2017). Thenoyltrifluoroacetone (TTA)-Carbon Dot/Aerogel Fluorescent Sensor for Lanthanide and Actinide Ions. *ACS Omega*, *2*(12), 9288–9295.

Ezati, P., Rhim, J. W., Molaei, R., Priyadarshi, R., Roy, S., Min, S., Kim, Y.H., Lee, S.G., & Han, S. (2022). Preparation and characterization of B, S, and N-doped glucose carbon dots: Antibacterial, antifungal, and antioxidant activity. *Sustainable Materials and Technologies*, *32*, e00397.

Franco, P., Aliakbarian, B., Perego, P., Reverchon, E., & De Marco, I. (2018). Supercritical adsorption of quercetin on aerogels for active packaging applications. *Industrial & Engineering Chemistry Research*, *57*(44), 15105-15113.

Gao, F., Ma, S., Li, J., Dai, K., Xiao, X., Zhao, D., & Gong, W. (2017). Rational design of high quality citric acid-derived carbon dots by selecting efficient chemical structure motifs. *Carbon*, *112*, 131-141.

Himaja, A. L., Karthik, P. S., & Singh, S. P. (2015). Carbon dots: the newest member of the carbon nanomaterials family. *The Chemical Record*, *15*(3), 595-615.

Hu, T., Xu, J., Ye, Y., Han, Y., Li, X., Wang, Z., Sun, D., Zhou, Y., & Ni, Z. (2019). Visual detection of mixed organophosphorous pesticide using QD-AChE aerogel based microfluidic arrays sensor. *Biosensors and Bioelectronics*, *136*, 112–117.

Hu, Y., Yang, J., Tian, J., Jia, L., & Yu, J. S. (2014). Waste frying oil as a precursor for one-step synthesis of sulfur-doped carbon dots with pH-sensitive photoluminescence. *Carbon*, *77*, 775-782.

Jing, L., Yang, S., Li, X., Jiang, Y., Lou, J., Liu, Z., Ding, Q., & Han, W. (2022). Effective adsorption and sensitive detection of Cr6+ by degradable collagen-based porous fluorescent aerogel. *Industrial Crops and Products*, *182*, 114882.

Jorns, M., & Pappas, D. (2021). A review of fluorescent carbon dots, their synthesis, physical and chemical characteristics, and applications. *Nanomaterials*, *11*(6), 1448.

Khairol Anuar, N. K., Tan, H. L., Lim, Y. P., So'aib, M. S., & Abu Bakar, N. F. (2021). A review on multifunctional carbon-dots synthesized from biomass waste: design/fabrication, characterization and applications. *Frontiers in energy research*, *9*, 626549.

Koshy, R. R., Koshy, J. T., Mary, S. K., Sadanandan, S., Jisha, S., & Pothan, L. A. (2021). Preparation of pH sensitive film based on starch/carbon nano dots incorporating anthocyanin for monitoring spoilage of pork. *Food Control*, *126*, 108039.

Kumar, Y., Singh, L., Sharanagat, V. S., Patel, A., & Kumar, K. (2020). Effect of microwave treatment (low power and varying time) on potato starch: Microstructure, thermo-functional, pasting and rheological properties. *International Journal of Biological Macromolecules*, *155*, 27-35.

Lu, W., Qin, X., Liu, S., Chang, G., Zhang, Y., Luo, Y., Asiri, A.M., Al-Youbi, A.O., & Sun, X. (2012). Economical, green synthesis of fluorescent carbon nanoparticles and their use as probes for sensitive and selective detection of mercury (II) ions. *Analytical chemistry*, *84*(12), 5351-5357.

Luo, Z., He, X., Fu, X., Luo, F., &Gao, Q. (2006). Effect of microwave radiation on the physicochemical properties of normal maize, waxy maize and amylomaize V starches. *Starch/Staerke*, *58*(9), 468–474.

Meierhofer, F., Dissinger, F., Weigert, F., Jungclaus, J., Müller-Caspary, K., Waldvogel, S. R., Resch-Genger, U., & Voss, T. (2020). Citric acid based carbon dots with amine type stabilizers: pH-specific luminescence and quantum yield characteristics. *The Journal of Physical Chemistry C*, *124*(16), 8894-8904.

MJ, P. D., Sangeeta, A., & Mishra, P. (2025). Development of Multifunctional C-dots from Processing Waste of Pomelo Fruits for Determination of pH and Methyl Parathion. *Journal of Fluorescence*, 1-13.

Mohammed, S. J., Omer, K. M., & Hawaiz, F. E. (2023). Deep insights to explain the mechanism of carbon dot formation at various reaction times using the hydrothermal technique: FT-IR, 13 C-NMR, 1 H-NMR, and UV-visible spectroscopic approaches. *RSC advances*, *13*(21), 14340-14349.

Moradi, M., Molaei, R., Kousheh, S. A., T. Guimarães, J., & McClements, D. J. (2021). Carbon dots synthesized from microorganisms and food by-products: active and smart food packaging applications. *Critical Reviews in Food Science and Nutrition*, 1-17.

Naksen, P., Jarujamrus, P., Anutrasakda, W., Promarak, V., Zhang, L., & Shen, W. (2022). Old silver mirror in qualitative analysis with new shoots in quantification: nitrogen-doped carbon dots (N-CDs) as fluorescent probes for "off-on" sensing of formalin in food samples. *Talanta*, *236*, 122862.

Ozyurt, D., Al Kobaisi, M., Hocking, R. K., & Fox, B. (2023). Properties, synthesis, and applications of carbon dots: A review. *Carbon Trends*, *12*, 100276.

Pappalardo, J. S., Macairan, J. R., Macina, A., Poulhazan, A., Quattrocchi, V., Marcotte, I., & Naccache, R. (2020). Effects of polydopamine-passivation on the optical properties of carbon dots and its potential use in vivo. *Physical Chemistry Chemical Physics*, *22*(29), 16595-16605.

Prinz, A. L., & Richter, D. J. (2022). Long-term exposure to fine particulate matter air pollution: an ecological study of its effect on COVID-19 cases and fatality in Germany. *Environmental research*, *204*, 111948.

Qu, D., Zheng, M., Zhang, L., Zhao, H., Xie, Z., Jing, X., Haddad, R.E., Fan, H., & Sun, Z. (2014). Formation mechanism and optimization of highly luminescent N-doped graphene quantum dots. *Scientific reports*, *4*(1), 5294.

Schaber, P. M., Colson, J., Higgins, S., Thielen, D., Anspach, B., & Brauer, J. (2004). Thermal decomposition (pyrolysis) of urea in an open reaction vessel. *Thermochimica acta*, *424*(1-2), 131-142.

Schneider, J., Reckmeier, C. J., Xiong, Y., von Seckendorff, M., Susha, A. S., Kasák, P., & Rogach, A. L. (2017). Molecular fluorescence in citric acid-based carbon dots. *The Journal of Physical Chemistry C*, *121*(3), 2014-2022.

Sharma, A., & Das, J. (2019). Small molecules derived carbon dots: synthesis and applications in sensing, catalysis, imaging, and biomedicine. *Journal of nanobiotechnology*, *17*(1), 92.

Sharshir, S. W., Algazzar, A. M., Elmaadawy, K. A., Kandeal, A. W., Elkadeem, M. R., Arunkumar, T., Zang, J., & Yang, N. (2020). New hydrogel materials for improving solar

water evaporation, desalination and wastewater treatment: A review. *Desalination*, *491*, 114564.

Sk, M. P., & Chattopadhyay, A. (2014). Induction coil heater prepared highly fluorescent carbon dots as invisible ink and explosive sensor. *RSC Advances*, *4*(60), 31994-31999.

Sun, J., Liu, Y., Wu, Z., Xu, M., Lei, E., Ma, C., Luo, S., Huang, J., Li, W., & Liu, S. (2021). Compressible, anisotropic lamellar cellulose-based carbon aerogels enhanced by carbon dots for superior energy storage and water deionization. *Carbohydrate Polymers*, *252*, 117209.

Tiwari, A., Walia, S., Sharma, S., Chauhan, S., Kumar, M., Gadly, T., & Randhawa, J. K. (2023). High quantum yield carbon dots and nitrogen-doped carbon dots as fluorescent probes for spectroscopic dopamine detection in human serum. *Journal of Materials Chemistry B*, *11*(5), 1029-1043.

Vallan, L., & Imahori, H. (2022). Citric acid-based carbon dots and their application in energy conversion. *ACS applied electronic materials*, *4*(9), 4231-4257.

Vervald, A. M., Laptinskiy, K. A., Khmeleva, M. Y., & Dolenko, T. A. (2025). Toward carbon dots from citric acid and ethylenediamine, part 1: Structure, optical properties, main luminophore at different stages of synthesis. *Carbon Trends*, *19*, 100452.

Wang, C., Hu, T., Wen, Z., Zhou, J., Wang, X., Wu, Q., & Wang, C. (2018). Concentration-dependent color tunability of nitrogen-doped carbon dots and their application for iron (III) detection and multicolor bioimaging. *Journal of colloid and interface science*, *521*, 33-41.

Wang, L., Wu, Q., Zhao, B., Li, Z., Zhang, Y., Huang, L., & Yu, S. (2022). Multi-functionalized carbon aerogels derived from chitosan. *Journal of Colloid and Interface Science*, *605*, 790-802.

Wang, N., Hei, Y., Liu, J., Sun, M., Sha, T., Hassan, M., Bo, X., Guo, Y., & Zhou, M. (2019). Low-cost and environment-friendly synthesis of carbon nanorods assembled hierarchical meso-macroporous carbons networks aerogels from natural apples for the electrochemical determination of ascorbic acid and hydrogen peroxide. *Analytica Chimica Acta*, *1047*, 36–44.

Wang, Ru, Lu, K. Q., Zhang, F., Tang, Z. R., & Xu, Y. J. (2018). 3D carbon quantum dots/graphene aerogel as a metal-free catalyst for enhanced photosensitization efficiency. *Applied Catalysis B: Environmental*, *233*, 11–18.

Wei, W., Huang, J., Gao, W., Lu, X., & Shi, X. (2021). Carbon dots fluorescence-based colorimetric sensor for sensitive detection of aluminum ions with a smartphone. *Chemosensors*, *9*(2), 25.

Wu, B., Zhu, G., Dufresne, A., & Lin, N. (2019). Fluorescent Aerogels Based on Chemical Crosslinking between Nanocellulose and Carbon Dots for Optical Sensor. *ACS Applied Materials and Interfaces*, *11*(17), 16048–16058.

Xiao, M., Xu, N., He, A., Yu, Z., Chen, B., Jin, B., Jiang, L., & Yi, C. (2023). A smartphone-based fluorospectrophotometer and ratiometric fluorescence nanoprobe for on-site quantitation of pesticide residue. *iScience*, *26*(4).

Xu, X., Chang, Q., Xue, C., Li, N., Wang, H., Yang, J., & Hu, S. (2022). A carbonized carbon dot-modified starch aerogel for efficient solar-powered water evaporation. *Journal of Materials Chemistry A*, *10*(21), 11712-11720.

Zattar, A. P. P., Fajardo, G. L., de Mesquita, J. P., & Pereira, F. V. (2021). Luminescent carbon dots obtained from chitosan: A comparison between different methods to enhance the quantum yield. *Fullerenes, Nanotubes and Carbon Nanostructures*, *29*(6), 414-422.

Zhang, M., Xue, J., Zhu, Y., Yao, C., & Yang, D. (2020). Multiresponsive white-light emitting aerogel prepared with codoped lanthanide/thymidine/carbon dots. *ACS Applied Materials & Interfaces*, *12*(19), 22191-22199.

Zhou, M., Zhou, Z., Gong, A., Zhang, Y., & Li, Q. (2015). Synthesis of highly photoluminescent carbon dots via citric acid and Tris for iron (III) ions sensors and bioimaging. *Talanta*, *143*, 107-113.

Zhu, Y., Yan, L., Xu, M., Li, Y., Song, X., & Yin, L. (2021). Difference between ammonia and urea on nitrogen doping of graphene quantum dots. *Colloids and Surfaces A: Physicochemical and Engineering Aspects*, *610*, 125703.